Angewandte Chemie

Eine Zeitschrift der Gesellschaft Deutscher Chemiker

www.angewandte.de

Akzeptierter Artikel

Titel: Designing Polymer-in-Salt Electrolyte and Fully Infiltrated 3D Electrode for Integrated Solid-State Lithium Batteries

Autoren: Wenyi Liu, Chengjun Yi, Linpo Li, Shuailei Liu, Qiuyue Gui, Deliang Ba, Yuanyuan Li, Dongliang Peng, and Jinping Liu

Zitierweise: *Angew. Chem. Int. Ed.* 10.1002/anie.202101537

Link zur VoR: https://doi.org/10.1002/anie.202101537

WILEY-VCH

10.1002/ange.202101537

WILEY-VCH

RESEARCH ARTICLE

Designing Polymer-in-Salt Electrolyte and Fully Infiltrated 3D Electrode for Integrated Solid-State Lithium Batteries

Wenyi Liu, Chengjun Yi, Linpo Li, Shuailei Liu, Qiuyue Gui, Deliang Ba, Yuanyuan Li, Dongliang Peng and Jinping Liu*

[*] W. Y. Liu, C. J. Yi, S. L. Liu, Q. Y. Gui and Prof. J. P. Liu
State Key Laboratory of Advanced Technology for Materials Synthesis and Processing and School of Chemistry, Chemical Engineering and Life Science
Wuhan University of Technology
Wuhan, Hubei 430070, P. R. China
E-mail: liujp@whut.edu.cn
L. P. Li, D. L. Ba and Prof. Y. Y. Li
School of Optical and Electronic Information
Huazhong University of Science and Technology
Wuhan 430074, P. R. China
Prof. D. L. Peng
State Key Lab of Physical Chemistry of Solid Surface, Fujian Key Laboratory of Materials Genome, Collaborative Innovation Center of Chemistry for Energy Materials, College of Materials
Xiamen University
Xiamen 361005, P. R. China

Supporting information for this article is given via a link at the end of the document.

Abstract: Solid-state lithium batteries (SSLBs) are very promising due to their enhanced safety and high energy density, but greatly plagued by the relatively low ionic conductivity of solid-state electrolytes and large electrolyte-electrode interfacial resistance. Herein, we design a poly(vinylidene fluoride-co-hexafluoropropylene) (PVDF-HFP)-based polymer-in-salt solid electrolyte (PISSE) with high room-temperature ionic conductivity (1.24×10^{-4} S cm^{-1}) and construct a model integrated TiO_2/Li SSLB with 3D fully infiltration of solid electrolyte. With forming aggregated ion clusters, unique ionic channels are generated in the PISSE, providing much faster Li^+ transport than common polymer electrolytes. Moreover, the integrated device simultaneously achieves maximized interfacial contact and electrochemical and mechanical stability, presenting high performance close to that with liquid electrolyte. A pouch cell made of 2 SSLB units in series shows high voltage plateau (3.7 V) and volumetric energy density comparable to many commercial thin-film batteries (microbatteries), which also exhibits robust flexibility and brilliant safety under abuse tests.

Introduction

Lithium (Li) metal with an extremely high theoretical capacity (3860 mAh g^{-1}) and the lowest redox potential (-3.04 V vs. the standard hydrogen electrode) has been regarded as a promising anode for next-generation high-energy batteries.[1-3] However, battery failure generally occurs due to parasitic reactions and anode pulverization, wherein liquid electrolytes (LEs) continuously react with Li metal.[4,5] The uncontrolled Li dendrites formed during electrochemical Li plating/stripping in LEs can also lead to battery short-circuit, impeding the practical application of Li metal anode in lithium batteries.[6,7] To address these issues, solid-state electrolytes are considered as particularly ideal replacements for the flammable LEs because of their inherent safety characteristics and potential to prevent dendritic deposition and structural damage of Li anode.[8-10]

Among all solid-state electrolytes, solid polymer electrolytes (SPEs) comprised of lithium salt and polymer are particularly attractive by virtue of their low cost, facile preparation, high flexibility and easiness of forming intimate interface with electrode.[11-13] Unfortunately, the ionic conductivity of SPEs at room temperature (RT) is generally low.[14,15] Considering that the ionic transport in SPEs is completed by the local relaxation and segmental motion of amorphous regions in polymer chains (**Figure 1**a),[16-18] various approaches, including cross-linking,[19,20] forming copolymer,[21] and introducing inorganic fillers,[22] have been implemented to expand the proportion of amorphous regions to promote ionic conductivity. Alternatively, polymer-in-salt solid electrolyte (PISSE: the content of the lithium salt exceeding 50 wt.%), despite being rarely investigated, has great potentials because it can achieve high ionic conductivity at RT via a facile and quite straightforward way.[23-25] In this system, the proportion of amorphous regions has been maximized due to the complete interaction between sufficient lithium salt and the polymer matrix. Besides, the transport of lithium ions is achieved not only by the movement of the amorphous regions of the polymer but also through the unique ionic channel constructed by ion clusters (Figure 1b).[24-26] Till now, a few polymer matrices,[25b,26-30] especially polycarbonates,[27] have been utilized in PISSEs with satisfactory ionic conductivity at RT. Nevertheless, their mechanical properties were deteriorated, which is caused by ultrahigh concentration of Li salt in PISSEs. Some attempts have been devoted to improving the mechanical properties of these PISSEs by incorporating extra additives with high mechanical strength,[27,28,31,32] such as active ceramic fillers[27] and cellulose acetate,[31] which however complicate the synthesis process. In principle, the simple and effective way to gain highly conductive PISSEs is to search for polymer matrices with excellent mechanical strength. Different from other polymers such as poly(ethylene oxide) (PEO), polyacrylonitrile (PAN) and polycarbonate[15,28,32b], poly(vinylidene fluoride-co-hexafluoropropylene) (PVDF-HFP) is expected to has superior comprehensive properties, as depicted in Figure 1c. It can not

10.1002/ange.202101537

only dissolve and dissociate large amounts of lithium salt to obtain high ionic conductivity at RT, but also have excellent mechanical strength, and thermal and electrochemical stability.[33] Despite these advantages, PVDF-HFP-based PISSEs have not yet been reported.

Besides the ionic conductivity of electrolytes, the interfacial issues between the solid electrolyte and electrode are also critical and challenging for solid-state Li batteries (SSLBs).[34,35] One issue at the interface is the interfacial instability caused by the redox reaction between the electrolyte and electrode especially at a high charge voltage or temperature, the other issue is a large interfacial impedance generated by the limited solid-solid rigid contact.[18,36] With electrochemically stable interface guaranteed, building an integrated electrode-electrolyte structure is of extreme importance to enhance interface affinity.[37] To this end, several previous studies have made attempts through directly casting SPEs onto the electrode surface or their mixed slurry, and fusing electrodes and electrolytes via heating or hot pressing.[36,38-41] Although the interfacial adhesion is reinforced, there remains critical challenges. These works used composite powder electrodes of active materials, electrolyte slurry and conductive additives, wherein active materials were wrapped with binders and conductive additives. Such an electrode will introduce random interfaces, which is not conducive to direct charge transfer because of increased ion/electron pathway. Besides, the electronic contact of these powder electrode-electrolyte structures with current collector is not easy to control, as SPEs introduce additional insulating phases into the electrode.[42a] To overcome the above dilemma, we proposed a unique solution of infiltrating polymer electrolytes into the interspacing of three-dimensional (3D) electrode grown directly on current collector, such as 3D nanoarrays (3D-NAs) architecture. In this design, 3D electrodes with no binders and additives can provide monophase and continuous 3D interfaces for achieving the most direct and sufficient contact with the SPE, ensuring much shortened ion transfer distance. In addition, the electronic conduction in the electrode can be ensured independently via straightforward transport along the continuous 3D framework and direct transfer at the electrode material-current collector interface.[42b] Notably, besides the potential application in common solid-state batteries, the 3D SSLBs are easy to be developed as thin-film batteries and wearable electronics and Internet of Things (IoT)[43]. Nevertheless, development of high-performance integrated 3D SSLBs with innovative SPEs and fully infiltrated architecture remains a huge challenge.

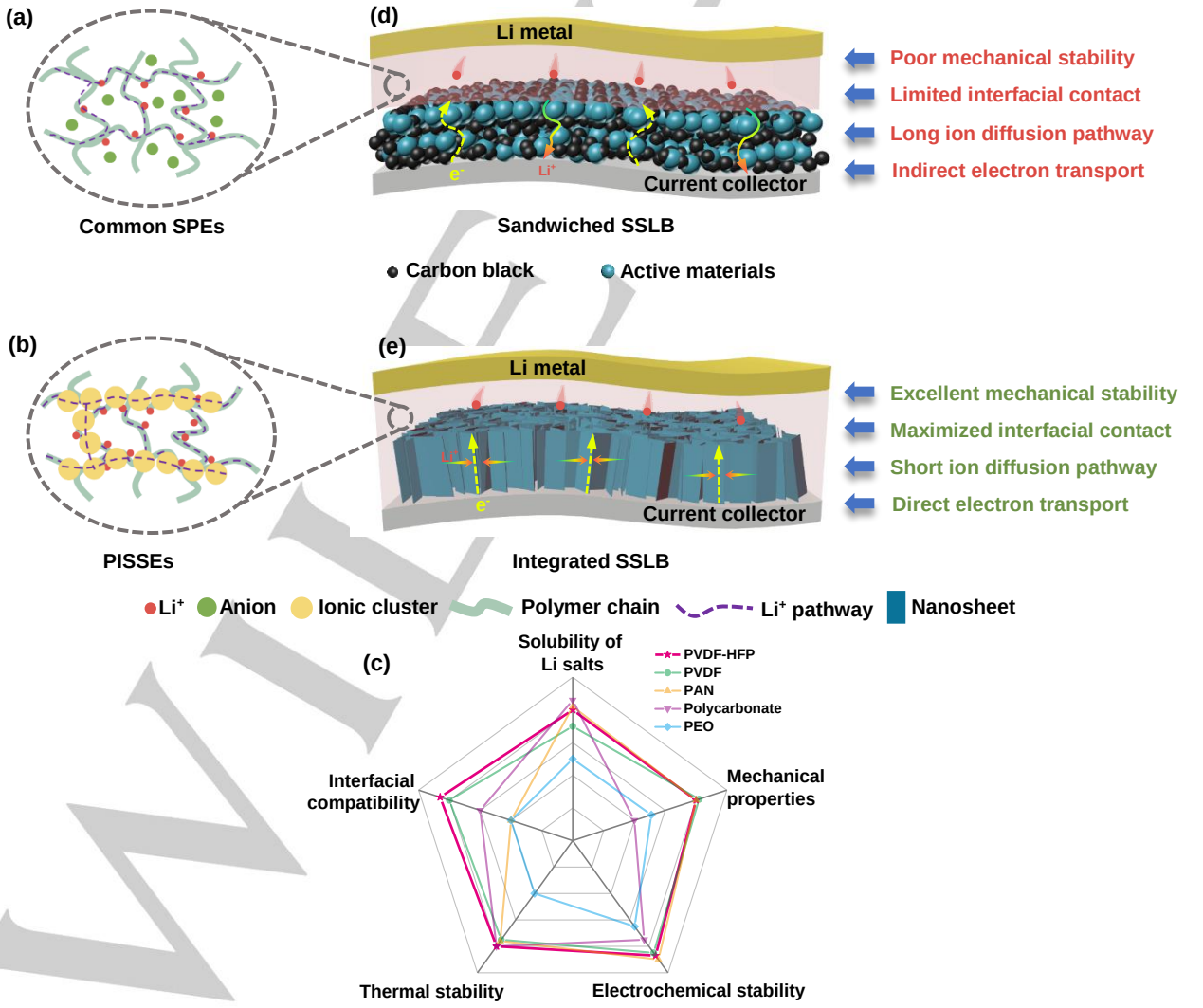

Figure 1. Schematic illustration of Li ion transport pathways in a) common SPEs and b) PISSEs. c) Radar plots that compare the properties of various polymer matrices. Schematic illustrations of d) sandwiched SSLBs and e) integrated SSLBs.

10.1002/ange.202101537

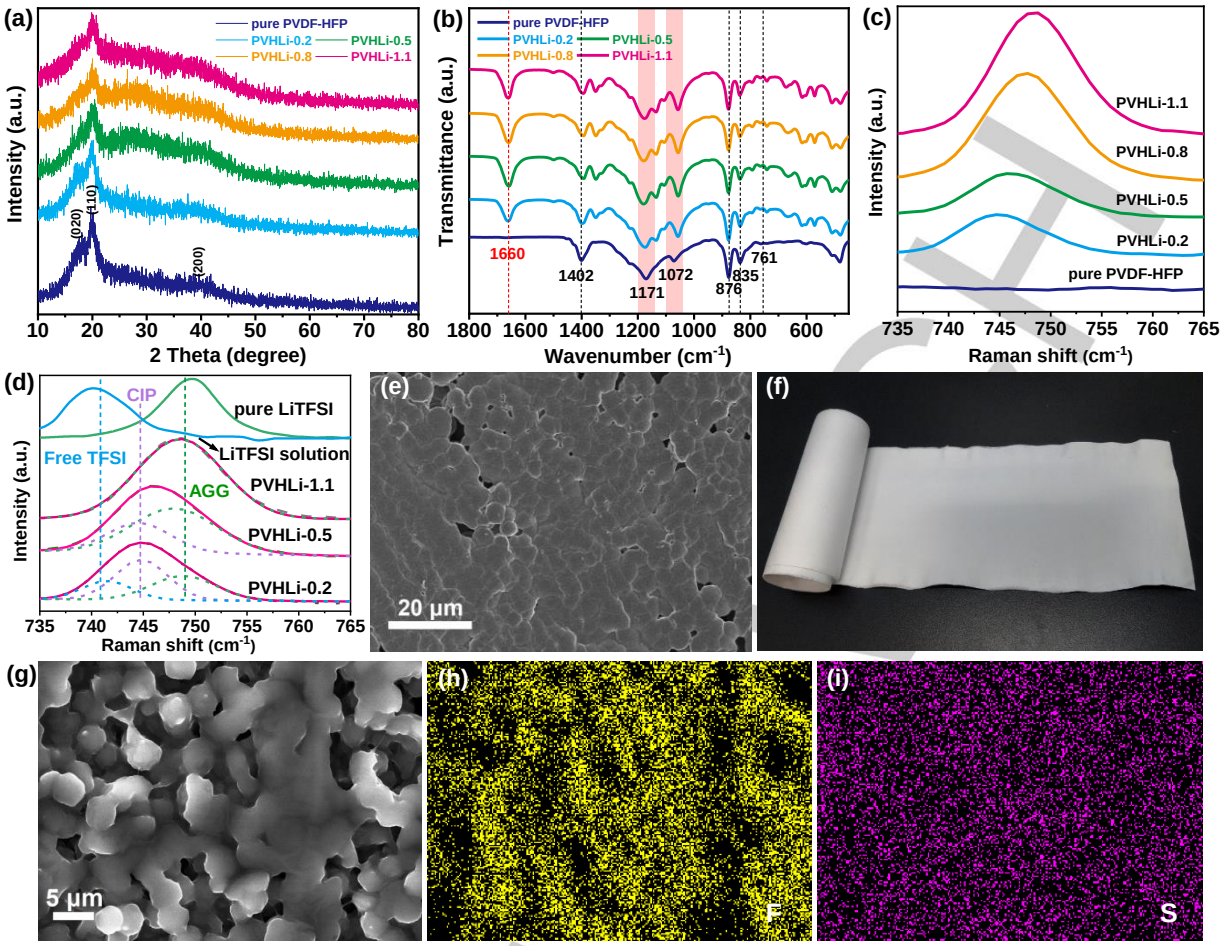

Figure 2. Characterizations of the polymer electrolyte membranes: a) XRD patterns and b) FTIR spectra of pure PVDF-HFP and PVHLi-x membranes. c) Raman spectra of $TFSI^-$ anion in different systems. d) Deconvolution of peaks of the S-N-S stretching vibrational mode (CIP: contact ion pair, AGG: aggregated ion pair). e) SEM image of the PVHLi-1.1 membrane. f) Photograph of a large-scale rolled-up PVHLi-1.1 membrane. g-i) EDS elemental mappings of F and S.

Herein, for the first time, we design a new kind of PISSE using PVDF-HFP as the matrix and assemble an integrated SSLB with a fully PISSE infiltrated 3D cathode. Compared to the conventional SSLBs (Figure 1d), our device (Figure 1e) possesses two main merits: 1) The PISSE based on PVDF-HFP, containing crystalline PVDF for maintaining the mechanical property of electrolyte and much F group for dissolving the numerous lithium salt, is designed without any fillers, cross-linkers and special microstructure tailoring, but exhibits high ionic conductivity at RT (1.24×10^{-4} S cm^{-1}) in the absence of free solvent. Moreover, owing to the wide electrochemical stable window of the PISSE (4.7 V vs. Li^+/Li), it enables high-voltage operation of the state-of-the-art $LiNi_{0.5}Co_{0.2}Mn_{0.3}O_2$ (NCM523) cathode; 2) Infiltrating PISSEs entirely into 3D electrode not only achieves maximized interfacial contact similar to the case with LEs, but also helps to maintain the stability of electrode and the whole device. In our work, TiO_2 is chosen as a model electrode material versus Li due to its low cost, nontoxicity, easy fabrication with 3D structure and outstanding electrochemical stability. In addition, simple packaging two of the TiO_2//Li cell in series can attain a high voltage comparable to that of commercial lithium ion batteries. As expected, our SSLB delivers a high reversible discharge capacity of 250 mAh g^{-1} at 0.1 C, excellent rate capability and good cycling stability; the comprehensive performance is even close to liquid Li battery counterpart and much better than corresponding SSLB with sandwich structure. The areal and volumetric performance is also comparable to commercial thin-film lithium microbatteries. A pouch cell made of 2 units in series exhibits a 3.7 V voltage plateau and can operate normally under different bending states and abuse testing (cut, puncture and fold), indicative of an excellent safety attribute.

Results and Discussion

Prior to the design of integrated electrode and device, PISSE was investigated in the form of membrane to understand the relationships between components and physical/chemical properties. Experimental section is provided in the Supporting Information. SPE membranes with different salt contents were prepared by a facile solution-casting method using N, N-dimethylformamide (DMF) as the solvent, marked as PVHLi-x (x=0.2, 0.5, 0.8, 1.1). To confirm the phase of the PVDF-HFP hosts, the X-ray diffraction (XRD) patterns were obtained and shown in **Figure 2**a. Characteristic peaks around 18°, 20°, and 40° are detected, which indicates that the PVDF-HFP matrix includesα-phase PVDF-HFP.[44] The position of each diffraction peak does not change but its intensity decreases, which demonstrates the increase of amorphous region after mixing with the bis(trifluoromethane)sulfonimide lithium (LiTFSI). These

10.1002/ange.202101537

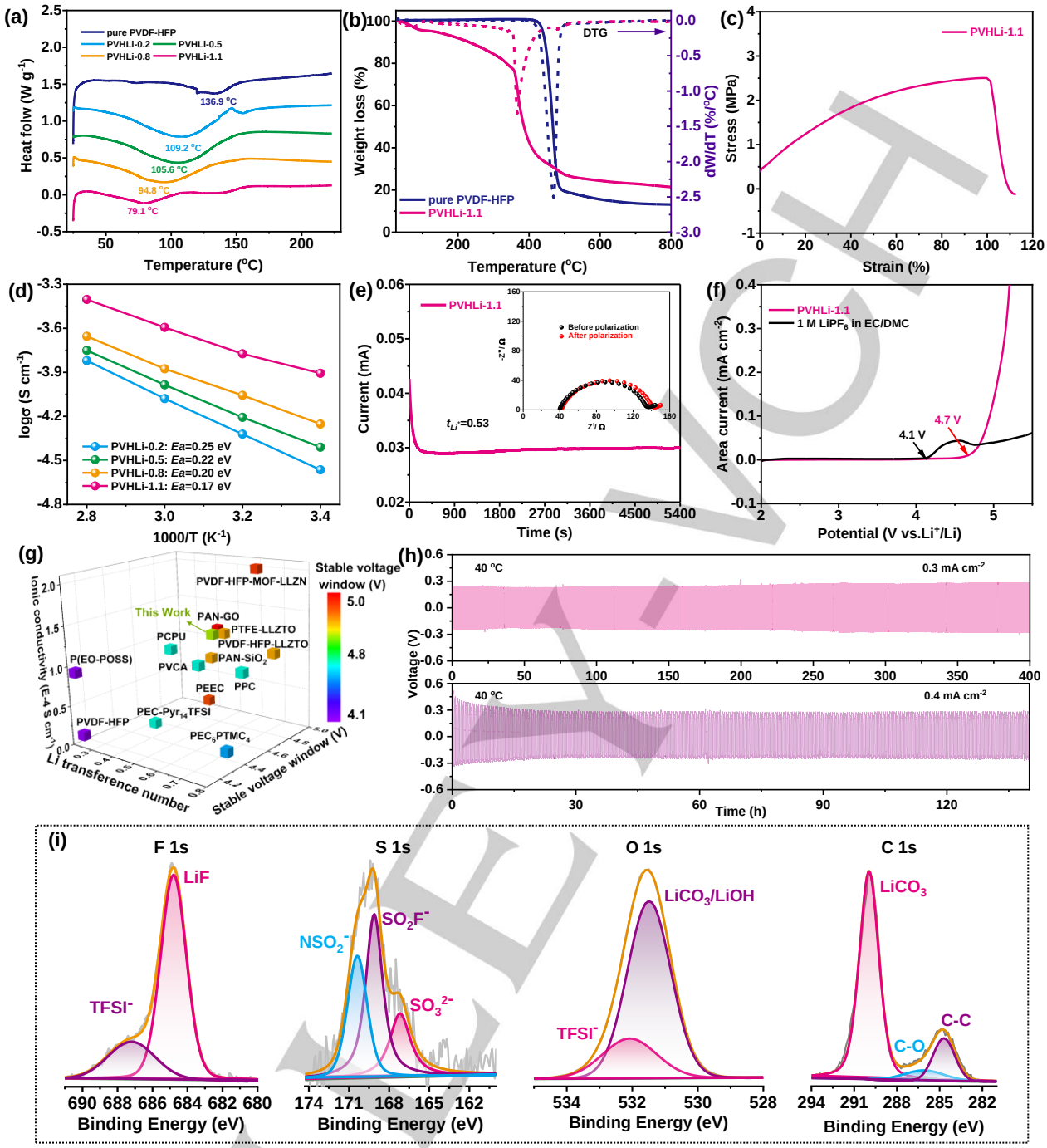

Figure 3. Physical and electrochemical properties of the polymer electrolyte membranes: a) DSC curves of PVHLi-x membranes. b) TGA and DTG curves of pure PVDF-HFP and PVHLi-1.1. c) Mechanical property of PVHLi-1.1. d) Arrhenius plots of the ionic conductivities of the PVHLi-X membranes. e) Polarization curve and impedance diagram of the cell before and after polarization (the inset) for PVHLi-1.1 at 25 ºC. f) LSV curves of PVHLi-1.1 membrane and LE at a scanning rate of 1 mV s^{-1} at 25 ºC. g) Comparison of PVHLi-1.1 with other reported polymer electrolytes. Some electrolytes that have conductivity higher than ours were generally designed with beneficial additives or special structural engineering. More details are provided in Table S3. h) Voltage profiles of the Li/PVHLi-1.1/Li battery at current densities of 0.3 and 0.4 mA cm^{-2}. i) XPS spectra of interface of the cycled Li metal in Li/PVHLi-1.1/Li battery (50 cycles).

confirm the role of LiTFSI in reducing the crystallinity of PVDF-HFP, thereby improving the ionic conductivity. The Fourier Transform infrared spectroscopy (FTIR) was used to identify the characteristic bands of salt and polymer, as well as interaction between them, as presented in Figure 2b. The characteristic peaks at 761 and 1402 cm^{-1} are assigned to α-phase crystal of PVDF-HFP, while the bands at 876 and 835 cm^{-1} are the amorphous phase.[45] The vibrations bands at 1072, 1171 cm^{-1} correspond to symmetrical stretching of CF_2, which are shifted after LiTFSI mixing, implying the interaction between PVDF-HFP matrix and LiTFSI.[46] Raman spectroscopy was used to further reveal intensified cation/anion interactions as salt concentration increases. As observed in Figure 2c and S1, the peak of $TFSI^-$ anion undergoes an upward shift as the salt concentration increases. The peak can be divided into three different dissociation states: free TFSI ions at 740 cm^{-1}, contact ion pairs

at 744 cm^{-1} (CIPs, TFSI ions interacting with a single Li ion), and aggregated ion pairs at 749 cm^{-1} (AGGs, TFSI ions interacting with two or more Li ions).[24] As demonstrated in the peak deconvolution results in Figures 2d, even in the PVHLi-0.2 electrolyte the majority of TFSI ions interact with one or more Li ions. Upon increasing the LiTFSI concentration, AGGs gradually predominates as the species of TFSI ion. When the weight ratio is up to 1.1, all the TFSI ions exist as AGGs. This phenomenon proves that cation/anion association enhances in high salt concentration,[47] forming unique and fast ion transport channels consisting of AGGs.

The scanning electron microscopy (SEM) images of pure PVDF-HFP and PVHLi-1.1 are displayed in Figure S2a and Figure 2e, respectively. Pure PVDF-HFP shows a densely connected spherical structure of several micrometers in diameter; while PVHLi-1.1 demonstrates a porous but interconnecting microstructure after free-solvent removal, which might aid ionic transport. The PVHLi-1.1 membrane displays good flexibility, is easy to roll up and can be fabricated on a large scale (Figure 2f, S2b and S2c). These results demonstrate the scalability of PVHLI-1.1 electrolyte and its potential to be used in flexible devices. The Energy-dispersive X-ray spectroscopy (EDS) mapping images of PVHLi-1.1 membrane (Figure 2g-i) further reveal that LiTFSI is evenly distributed in the PVDF-HFP backbone, which is crucial to guarantee the rapid Li^+ transport as well as good mechanical robustness of PISSE.

To determine the optimized value of *x* for PISSE, the glass transportation temperature (T_g) of pure PVDF-HFP and PVHLi-x electrolyte membranes with various salt concentrations was firstly tested. As displayed in **Figure 3**a, the T_g continuously decreases as LiTFSI content increasing. The T_g of PVHLi-1.1 is 79.1 ºC, much lower than that of pure PVDF-HFP and other electrolytes. This phenomenon is owing to the plasticizing effect of the large anion $TFSI^-$.[28] This further indicates that LiTFSI manages to inhibit the crystallinity of PVDF-HFP and enhance segmental movement of PVDF-HFP, which will be good for enhancing ion transport. The PVHLi-1.1 also demonstrates good thermal stability, as evidenced by thermos gravimetric analysis (TGA) and differential thermogravimetry (DTG). As shown in Figure 3b, the decomposition of polymer and salts in PVHLi-1.1 starts at ~320 ºC, while the initial decomposition of pure PVDF-HFP occurs at ~410 ºC. This should be ascribed to reduced crystallinity of PVDF-HFP matrix due to the interacting between the high concentrations of LiTFSI and PVDF-HFP, which probably makes the peak of PVDF-HFP overlap with that of LiTFSI in DTG curve. Nonetheless, PVHLi-1.1 membrane is thermally stable enough for SSLBs considering the stability up to 320 ºC. The minor weight loss of PVHLi-1.1 before 150 ºC is due to the trapped moisture.[48] The weight loss observed at 150-200 ºC derives from the evaporation of residual DMF. ^{1}H nuclear magnetic resonance (NMR) spectrum indeed demonstrated that the PVHLi-1.1 membrane contains DMF (Figure S3a). However, the TGA isotherm showed an overall solvent loss of only ~13 wt% (Figure S3b). More importantly, no Raman and FITR signal from free DMF was observed in PVHLi-x electrolyte membranes (Figure S3c-d), suggesting that these electrolyte membranes do not contain free solvent and the residual DMF exists in the bound form.[49] This is exactly the reason why our PISSE is still solid-state. Moreover, the mechanical behavior of PVHLi-1.1 was tested and shown in Figure 3c. Despite that the content of salt exceeds that of polymer in PISSEs, the mechanical properties are still acceptable. Tensile strength and strain at break of PVHLi-1.1 membrane are 2.5 MPa and 112%, respectively, absolutely potential for SSLBs.

To highlight the priority of PVHLi-1.1 in ionic conductivity, the influence of Li salt concentration on ionic conductivity of PVHLi-x electrolyte was investigated. Figure S4a illustrates the Nyquist plots of samples with different LiTFSI contents. An equivalent circuit model was used for fitting the impedance to extract the resistance of each sample (*R*). The ionic conductivity was calculated based on Equation 1 in Experimental section (Figure S4b). The ionic conductivity increases with increasing LiTFSI weight ratio from 0.2 to 0.8, which is attributed to increased carrier concentrations and decreased crystallinity of PVDF-HFP. When the weight ratio is up to 1.1, the ionic conductivity of the PVHLi-x electrolyte reaches as high as ca. 1.24×10^{-4} S cm^{-1} at 25 ºC. Compared to the low Li salt concentration SPEs with low ionic conductivities arising merely from the segmental polymer chains (associate with and dissociate from Li^+), the ionic conductivity in PISSEs significantly benefits from the motion of Li^+ through fast ion transport channels created by aggregated cation/anion clusters.[24,25,50] The activation energy (E_a) of different PVHLi-x electrolytes was calculated by the Arrhenius formula and listed in Table S1. Because of the least resistance to segmental motion and unique Li^+ transport pathway in PISSEs, the PVHLi-1.1 has the lowest migration barrier for ion transport. It exhibits the lowest E_a (0.17 eV) among tested electrolytes, suggesting that high content of lithium salt can reduce the E_a of lithium ion migration. As further seen in Figure 3d and Figure S5a, the PVHLi-1.1 always has the highest ionic conductivity in the temperature range of 25-80 ºC and the ionic conductivity rises with temperature increasing, which follows an Arrhenius behavior. It was found that the ionic conductivity was improved when the weight ratio reached 1.3 in PISSE. However, the mechanical property significantly deteriorated (Figure S5b). Based on the above discussion, we chose PVHLi-1.1 with x=1.1 as the optimized PISSE for next investigations.

LiTFSI plays an important role in the formation of high-conductivity PISSE. To confirm this, other two anionic salts were tested with the same salt concentration as PVHLi-1.1 for comparison ($LiClO_4$-based PISSE was defined as PVHCl-1.1, and $LiPF_6$-based one was defined as PVHPf-1.1). It can be seen from Figure S6 that PVHLi-1.1 shows the smallest impedance and the highest ionic conductivity at different temperatures. This is due to the delocalization of large anion $TFSI^-$ in LiTFSI, which makes LiTFSI the easiest to dissolve and dissociate in the polymer matrix than $LiPF_6$ and $LiClO_4$ at high content. While the interaction between the PVDF-HFP matrix and Li^+ cannot reach saturation state, there are no unique ion transport channels in PVHPf-1.1 and PVHCl-1.1 electrolytes. Besides, undissolved salt in them will hinder ions transference, resulting in lower ionic conductivity, especially at RT. Consistent with the above results, PVHLi-1.1 shows the lowest E_a (Table S2), which again indicates that LiTFSI is more suitable for PVDF-HFP-based PISSEs than other Li salts. Lithium transference number (t_{Li^+}) in SPE is another crucial factor to evaluate the mobility of Li ions. The solid electrolyte with high t_{Li^+} can achieve a uniform migration and deposition of Li^+.[51] The potentiostatic polarization method was used to obtain the t_{Li^+} of the PVHLi-1.1 electrolyte, with electrochemical impendence spectroscopy (EIS) measurements performed immediately before and after a small polarization was applied to a Li/Li symmetric cell.

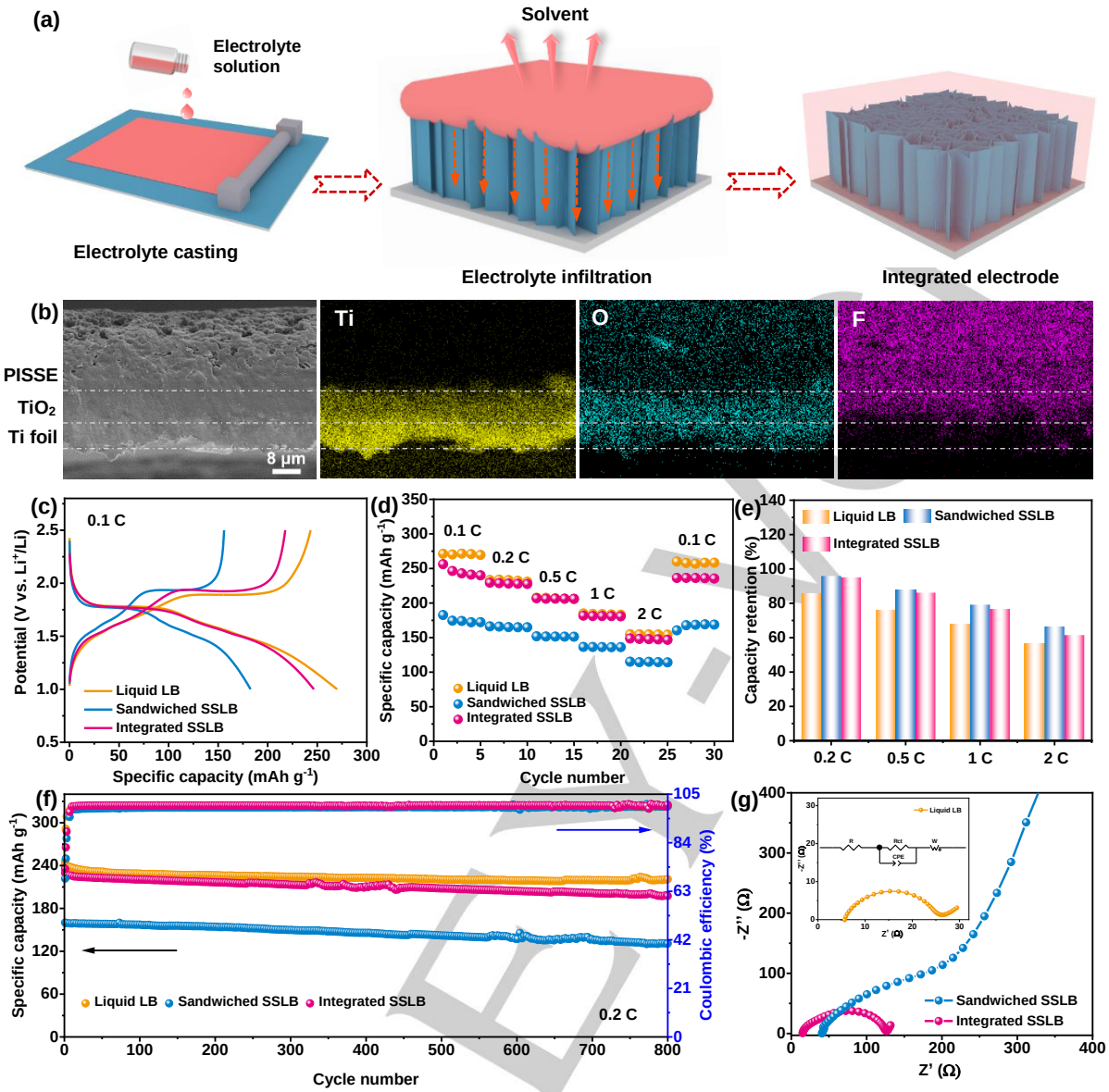

Figure 4. a) Schematic of the preparation process of 3D integrated electrode. b) EDS mappings of Ti, O and F in the cross section of the integrated 3D electrode. Electrochemical performances of the assembled SSLBs at 25 °C: c) Charge-discharge curves at 0.1 C. d) Rate performances and e) corresponding capacity retention. f) Cycling performance at 0.2 C and g) electrochemical impedance plots of the devices.

From the direct-current (DC) polarization results, t_{Li}^+ of PVHLi-1.1 is calculated to be 0.53 based on the Bruce-Vincent-Evans equation (Figure 3e), which is higher than that of the traditional organic liquid electrolytes (0.38) and the typical SPEs.[52] The high t_{Li}^+ of PVHLi-1.1 can be attributed to the fact that besides $TFSI^-$ anion is too large to freely migrate, its migration is further limited due to the interaction with PVDF-HFP. More importantly, the formation of aggregated ionic clusters can restrict the movement of $TFSI^-$ and rapidly transport Li^+.[25,30]

In addition to high ionic conductivity and good t_{Li}^+, PVHLi-1.1 electrolyte membrane possesses good electrochemical stability. In the linear sweep voltammetry (LSV) measurements (Figure 3f and S7), a mild current peak is observed at 4.1 V for the liquid electrolyte, while the PVHLi-1.1 is stable up to 4.7 V without obvious current fluctuation. The result suggests that the PVHLi-1.1 electrolyte is more electrochemically stable than liquid electrolyte, which can be attributed to the good electrochemical stability of pristine PVDF-HFP matrix, and the interaction between the high content LiTFSI and PVDF-HFP that further inhibits decomposition of PVDF-HFP under high voltage. Thus, the electrochemical stability window of the PVHLi-1.1 electrolyte is wide enough to meet the requirements of most prime cathode candidates for Li batteries. To explore the stabilizing effect of PVDF-HFP on LiTFSI of high concentration, we tested the ionic conductivities of casted membranes whose precursor solution of PVHLi-1.1 was stored for different times (Figure S8; purple). The ionic conductivity can still maintain order of magnitude of 10^{-4} after even four weeks of storing of the precursor solution, different from some previous PISSEs (ionic conductivity decreased due to the salt precipitation).[53] The ionic conductivity of electrolyte membrane was also stable when sealed in ziplock bag and stored (Figure S8; red). Figure 3g and Table S3 show the detailed comparison of our new PISSE with many kinds of previously reported polymer electrolytes. It is quite encouraging that without

10.1002/ange.202101537

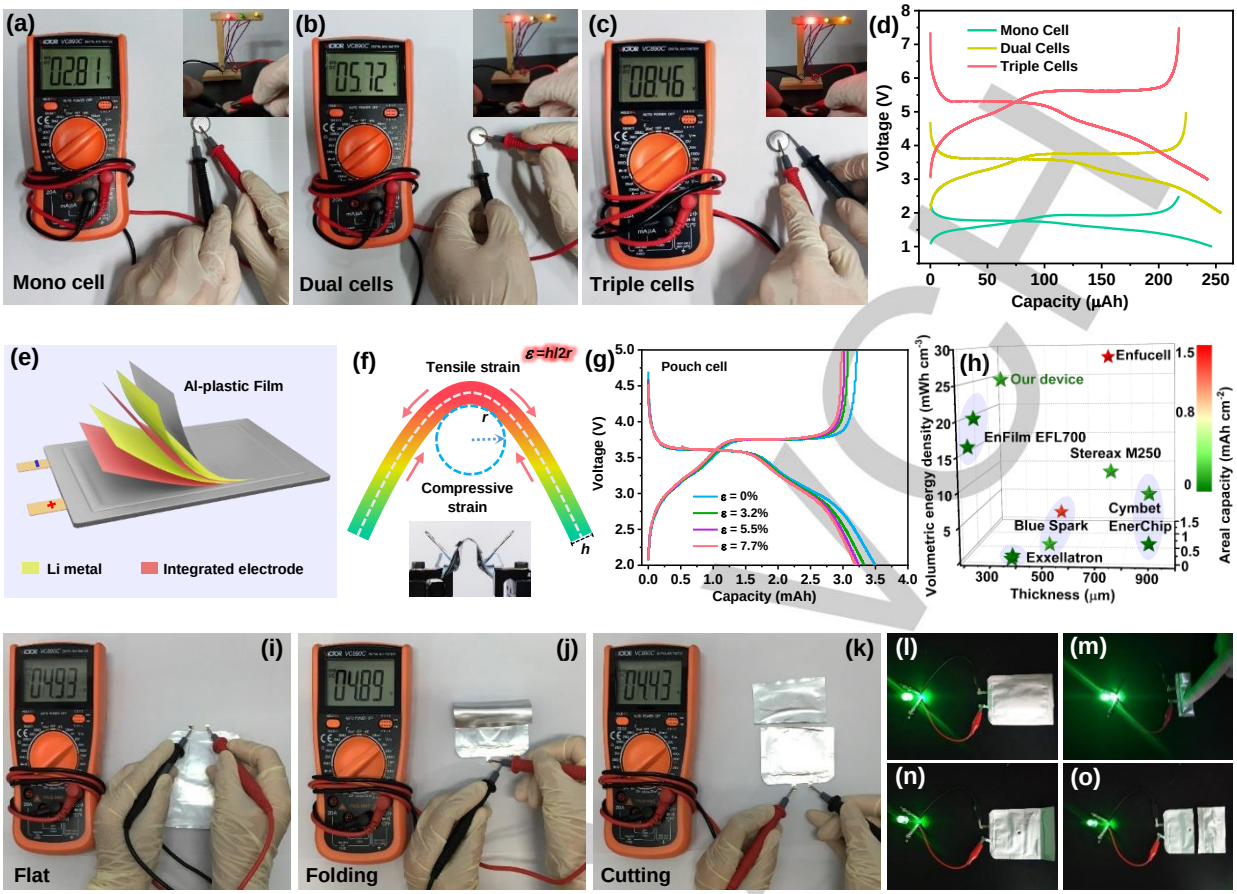

Figure 5. a-c) Voltages of open circuits of a SSLB unit, 2 SSLB units and 3 SSLB units. All mono/dual/triple cells can power LEDs in series (inset). d) Voltage profiles of SSLBs from 1 to 3 cells in series at 0.1 C. e) Schematic illustration of the flexible pouch cell packaged in series. f) Schematic description of the bending state of pouch cell. g) Voltage profiles of the pouch cell at 0.1 C under different bending states. h) Comparison of our device with commercial thin-film Li batteries and microbatteries. More details are provided in Table S5. i-k) Open-circuit voltages of the pouch cell under different states. l-o) Optical images of the pouch cell lighting a green LED under different states.

using any fillers, cross-linkers and special microstructure engineering, the designed PVHLi-1.1 exhibits attractive comprehensive attributes in terms of ionic conductivity at RT, t_{Li}^{+} and voltage window in the absence of free solvents. In particular, the performance of our PVHLi-1.1 is among the best reported for PISSEs.

The voltage profiles of Li plating/stripping cycling in the symmetric Li/PVHLi-1.1/Li cells at various current densities with periodically charged/discharged for 0.5h are presented in Figure 3h and S9 to probe the interfacial stability (safety) against Li anode. The polarization increases with the current density increases, but the polarization voltage can remain stable without a short-circuit at various current densities (0.01-0.4 mA cm^{-2}). Even cycling 400 times at the large current density of 0.3 mA cm^{-2}, the polarization voltage still keeps stable without obvious fluctuation, indicating that PVHLi-1.1 is compatible with Li metal. The critical current density was measured to be 0.5 mA cm^{-2}. The morphology of Li metal after 50 cycles is given in Figure S10. Obviously, the relatively smooth Li surface without any detectable dendrite structure is observed, demonstrating the effectiveness of our PISSE in preventing lithium dendrite growth. To clarify the cycling stability resulting from the solid electrolyte and interfacial engineering, the compositions of the interface layers from the cycled Li metal surface was investigated by X-ray photoelectron spectroscopy (XPS). XPS spectra of F, S, O and C are presented in Figure 3i. The interfacial layer formed on Li anode mainly consisted of LiF, Li_2CO_3, LiOH and sulfur compounds, mainly attributed to the interfacial reaction between $TFSI^-$ and Li metal. This multicomponent interface layer delivered promising ionic conductivity, excellent electronic insulation, and good mechanical property, which should be responsible for the suppressed side reactions and sustainable lithium plating/stripping.[44,54]

The PVHLi-1.1 PISSE also enabled the high-voltage operation (~4.3 V) of commercial NCM523 cathode. As shown in Figure S11a-d, solid-state sandwiched NCM/PVHLi-1.1/Li batteries were assembled and tested in terms of galvanostatic charge-discharge, rate performance and cycling stability. The performance of conventional NCM/LE/Li cell was also included for comparison. The charge and discharge curves at a wide rate range of 0.2-5 C of the NCM/PVHLi-1.1/Li generally demonstrate well-defined plateaus similar to NCM/LE/Li. In particular, the capacity retention of NCM/PVHLi-1.1/Li cell is as high as 93.2% after 200 cycles at 1C while that of NCM/LE/Li cell is 88.8%, which is due to the aforementioned higher electrochemical stability window of our PVHLi-1.1 electrolyte than commercial LE. Compared with the NCM/LE/Li cell, the solid-state cell has lower discharge capacities and larger polarizations, especially at high rates. This is because the ionic conductivity limitation of solid-

state PVHLi-1.1 at RT and poor solid-solid interfacial contact between NCM and solid electrolytes. Nevertheless, the electrochemical performances of our NCM/PVHLi-1.1/Li outperform most of the recently reported NCM-based SSLBs using polymer electrolytes, ceramic/sulfide electrolytes or hybrid electrolytes with complicated design (Table S4), highlighting the superiority of our PISSE in enduring high voltage, being compatible with cathode and achieving stable interfacial stability.

Interface design is of great importance for SSLBs. Next, we will show that employing 3D electrode architecture and infiltrating SPEs into 3D electrode are very promising to maximize the interfacial contact and develop advanced SSLBs. We will present the first example of PISSE-based 3D integrated SSLB using TiO_2 as a model electrode versus Li. The 3D TiO_2 nanoarrays were fabricated on ultrathin Ti foil via a simple alkaline hydrothermal route and subsequent ion-exchange reaction. SEM and Transmission electron microscopy (TEM) images indicate the interconnected nanosheet structure of the array electrode. Meanwhile, the component is verified to be anatase TiO_2 by XRD and XPS measurements (Figure S12-S13 and detailed discussion in Figure captions).[55] Different from traditional powder electrode, 3D electrode grown directly on current collector not only ensures direct electron transport and shortened ion pathway, but also provides sufficient void spaces, which were naturally used to form an integrated electrode via PVHLi-1.1 infiltration. The integrated electrode was prepared by casting PVHLi-1.1 precursor solution onto the TiO_2 electrode. With the precursor solution infiltration at 60 °C, followed by electrically blowing and drying in vacuum, the electrolyte entered into the gap of nanoarrays and formed membrane, as schematically illustrated in **Figure 4**a. This infiltration has been facilitated by the good wettability of electrolyte precursor solution on 3D TiO_2 surface (Figure S14). Cross-sectional SEM image and EDS elemental mappings in Figure 4b unambiguously demonstrate that the Ti current collector, the 3D TiO_2 layer, and the solid PVHLi-1.1 layer are well integrated without any visible delamination, forming a 3D throughout contact between the electrode and electrolyte (the element F belongs to PVHLi-1.1).

To evaluate the lithium storage performance of 3D integrated SSLB, the assembled coin cells of TiO_2/PVHLi-1.1/Li were galvanostatically charged and discharged between 1.0 and 2.5 V at 25 °C. Liquid LB using commercial liquid electrolyte and sandwiched SSLB using PISSE membrane were also investigated for comparative studies. Typical charge-discharge curves of the three cells at 0.1 C are illustrated in Figure 4c. The sandwiched SSLB can only achieve discharge capacity of 182.7 mAh g^{-1}, while the integrated SSLB can deliver discharge capacity of 246.6 mAh g^{-1}, which is closer to liquid LB (270 mAh g^{-1}). In addition, the integrated SSLB exhibits a lower polarization voltage than the sandwiched one. These results clearly indicate the benefits of much increased contact area between electrode materials and electrolyte, which reduces the interfacial resistance due to the shortened ion transport length and enhances the materials utilization. Similarly, the discharge capacities of integrated SSLB are always larger than those of the sandwiched SSLB at all tested rates ranging from 0.1-2 C. It demonstrates excellent rate capability comparable to liquid LB, with capacities approaching to that of liquid LB at rates of 0.2-2 C. The capacity retention is 61.5% when the rate is increased by 20 times to 2 C (Figure 4d,e). Meanwhile, the cycling performance of our integrated SSLB is good. After 800 cycles at 0.2 C, the capacity remains 197.5 mAh g^{-1} with an excellent capacity retention of 86.8% (Figure 4f and S15). It is believed that the penetrated solid PVHLi-1.1 has also helped to stabilize the structural volume change of TiO_2 during cycling via confinement effect.[42] To directly verify the improvement of the interface contact by using an integrated architecture instead of the sandwiched configuration, EIS of the three cells before and after three cycles was conducted, and the Nyquist plots are shown in Figure 4g and S16, respectively. Indeed, the integrated SSLB exhibits both smaller bulk resistance and charge transfer resistance than the sandwiched SSLB. Considering the Li anode side is completely the same for the three cells, these resistance differences are essentially related to the TiO_2 side. Thus, it is concluded that for a given SPE with acceptable ionic conductivity, the SSLB performance can be significantly boosted by promoting the interfacial contact in an advanced battery structure.

Our 3D integrated SSLB demonstrates excellent stackable feature, which leads to a higher output voltage and thus a higher energy. To visually manifest this unique advantage, a battery pack made of 2 or 3 SSLB units in series was assembled and integrated in a coin type cell. As illustrated in **Figure 5**a-c, the voltage of open circuits (VOCs) of a SSLB unit, 2 SSLB units and 3 SSLB units is measured to be 2.81, 5.72, and 8.46 V, respectively. The galvanostatic charge/discharge profiles in Figure 5d further revealed that the change in capacity is negligible when connected in series but the plateau voltage of two and three packaged SSLBs is about 2 and 3 times that of a single SSLB, proving that the voltage increases linearly with the number of battery units in series. Three light-emitting diodes (LEDs: red, green, yellow) in series can be lit by our SSLB, and the brightness apparently increases with increasing the voltage of SSLBs.

In order to verify the application feasibility of the PVHLi-1.1 electrolyte and the potential of our 3D integrated SSLB, we further fabricated a flexible pouch cell by packaging two SSLB units in series (Figure 5e). Considering that cell failure during flexing is dominated by the strain applied on the cell components, which depends on not only bending radius (r) but also the cell thickness (h), the tensile strain ($\varepsilon=h/2r$) was used to evaluate the flexibility of the pouch cell (Figure 5f). As shown in Figure 5g, the assembled cell can operate well between 2.0-5.0 V with plateaus at ~3.7 V. The charge and discharge profiles as well as the capacity are almost unchanged under different bending states; there are still 91.53% capacity retained for the cell undergoing the biggest ε of 7.7 % (Figure S17). The tensile strain value of > 5% indicates that our device meets the bending requirement of the majority of wearable electronics.[56] In addition, when compared to state-of-the-art commercial thin-film batteries or microbatteries (nine kinds from different companies like EnFilm and Stereax), our integrated SSLB device manifests superior performance in terms of capacity, footprint, thickness, voltage and volumetric energy density (Table S5, Figure 5h). With the thickness of only 320 μm, it can achieve a capacity of 3.5 mAh with the footprint of 35 × 40 mm^2 and volumetric energy density of 25.46 mWh cm^{-3}. Solid-state electrolytes infiltrated into 3D electrode also endow the device with good safety, which cannot be guaranteed if using liquid and gel polymer electrolytes. As illustrated in Figure 5i-k, the open-circuit voltage of our assembled SSLB has no significant decrease in the folding and cutting experiments. Furthermore, even after severe folding, puncturing and cutting tests, the device can light up a LED with strong luminescence, as displayed in

Figure 5l-o. A Video demonstrating the ability of our device in enduring these abuse tests is provided in Supporting Information.

Conclusion

In summary, we successfully designed a PVDF-HFP-based PISSE and constructed an integrated SSLB realized via entirely infiltrating PISSE into 3D TiO_2 electrode. In this integrated SSLB, the PISSE delivered high room-temperature ionic conductivity and Li ion transference number. Meanwhile, such an integrated design can significantly improve the solid-solid electrode/electrolyte interfacial contact, supplying more percolation sites and channels for fast ion transport, and also can stabilize the structural volume change of the 3D electrode during cycling via confinement effect. Benefiting from these merits, integrated SSLBs exhibit higher capacity (246.6 mAh g^{-1}), superior rate performance and cycling performance compared to sandwiched SSLBs. The pouch cell made of 2 units in series showed robust flexibility with no obvious electrochemical performance degradation under different bending states, and indicated an excellent safety behavior after abuse tests without an internal short circuit or burning, implying great potential in practical applications. This study is anticipated to shed light on designing high-performance SPEs and solving interfacial issues in SSLBs using SPEs, and thus promotes the development of SSLBs.

Acknowledgements

This work was supported by grants from the National Key R&D Program of China (Grant No. 2016YFA0202602), the National Natural Science Foundation of China (Grant Nos. 51972257, 52072136 and 51872104) and the Natural Science Foundation of Hubei Province (2018CFB581).

Keywords: polymer-in-salt electrolytes • 3D electrolyte infiltration • interfacial engineering • solid-state lithium batteries • nanostructured thin-film batteries

References

[1] a) M. Armand, J. M. Tarascon, *Nature* **2008**, *451*, 652; b) Z. Gao, H. Sun, L. Fu, F. Ye, Y. Zhang, W. Luo, Y. Huang, *Adv. Mater.* **2018**, *30*, 1705702.

[2] a) R. S. Chen, Q. G. Li, X. Q. Yu, L. Q. Chen, H. Li, *Chem. Rev.* **2020**, *120*, 6820; b) P. Jaumaux, Q. Liu, D. Zhou, X. Xu, T. Wang, Y Wang, F. Kang, B. Li, G. Wang, *Angew. Chem. Int. Ed.* **2020**, *59*, 9134.

[3] a) J. Zhu, X. Li, C. Wu, J. Gao, H. Xu, Y. Li, X. Guo, H. Li, W. Zhou, *Angew. Chem. Int. Ed.* **2020**, *59*, 2; b) G. Xi, M. Xiao, S. Wang, D. Han, Y. Li, Y. Meng, *Adv. Funct. Mater.* DOI: 10.1002/adfm.202007598.

[4] a) Q. Zhao, X. T. Liu, S. Stalin, K. Khan, L. A. Archer, *Nat. Energy* **2019**, *4*, 365; b) K. Pan, L. Zhang, W. Qian, X. Wu, K. Dong, H. Zhang, S. Zhang, *Adv. Mater.* **2020**, *32*, 2000399.

[5] a) F. Q. Liu, W. P. Wang, Y. X. Yin, S. F. Zhang, J. L. Shi, L. Wang, X. D. Zhang, Y. Zheng, J. J. Zhou, L. Li, Y. G. Guo, *Sci. Adv.* **2018**, *4*, eaat5383; b) J. Wu, S. Liu, F. Han, X. Yao, C. Wang, *Adv. Mater.* DOI: 10.1002/adma.202000751.

[6] J. Y. Wan, J. Xie, X. Kong, Z. Liu, K. Liu, F. F. Shi, A. Pei, H. Chen, W. Chen, J. Chen, X. K. Zhang, L. Q. Zong, J. Y. Wang, L. Q. Chen, J. Qin, Y. Cui, *Nat. Nanotechnol.* **2019**, *14*, 705; b) S. Lou, F. Zhang, C. Fu, M. Chen, Y. Ma, G. Yin, and J. Wang, *Adv. Mater.* DOI: 10.1002/adma.202000721.

[7] a) L. Ma, S. Chen, X. Li, A. Chen, B. Dong, C. Zhi, *Angew. Chem. Int. Ed.* **2020**, *59*, 23836; b) K. B. Hatzell, X. C. Chen, C. L. Cobb, N. P. Dasgupta, M. B. Dixit, L. E. Marbella, M. T. McDowell, P. P. Mukherjee, A. Verma, V. Viswanathan, A. S. Westover, W. G. Zeier, *ACS Energy Lett.* **2020**, *5*, 922.

[8] a) T. F. Miller, 3rd, Z. G. Wang, G. W. Coates, N. P. Balsara, *Acc. Chem. Res.* **2017**, *50*, 590; b) Q. Xia, S. Sun, J. Xu, F. Zan, J. Yue, Q. Zhang, L. Gu, H. Xia, *Small*, **2018**, *14*, 1804149.

[9] a) J. Wang; G. Huang, K. Chen, X. Zhang, *Angew. Chem. Int. Ed.* **2020**, *59*, 9382; b) T. Famprikis, P. Canepa, J. A. Dawson, M. S. Islam, C. Masquelier, *Nat. Mater.* **2019**, *18*, 1278; b) C. Zhao, Q. Zhao, X. Liu, J. Zheng, S. Stalin, Q. Zhang, and L. A. Archer, *Adv. Mater.* **2020**, *32*, 1905629.

[10] a) Z. Y. Zou, Y. J. Li, Z. H. Lu, D. Wang, Y. H. Cui, B. K. Guo, Y. J. Li, X. M. Liang, J. W. Feng, H. Li, C. W. Nan, M. Armand, L. Q. Chen, K. Xu, S. Q. Shi, *Chem. Rev.* **2020**, *120*, 4169; b) J. Zhu, M. Yao, S. Huang, J. Tian, Z. Niu, *Angew. Chem. Int. Ed.* **2020**, *59*, 16480.

[11] K. Terabe, T. Hasegawa, T. Nakayama, M. Aono, *Nature* **2005**, *433*, 47.

[12] M. Liu, Z. Cheng, S. Ganapathy, C. Wang, L. A. Haverkate, M. Tułodziecki, S. Unnikrishnan, M. Wagemaker, *ACS Energy Lett.* **2019**, *4*, 2336.

[13] Y. Yao, Z. Wei, H. Wang, H. Huang, Y. Jiang, X. Wu, X. Yao, Z. S. Wu, Y. Yu, *Adv. Energy Mater.* **2020**, *10*, 1903698.

[14] T. Jiang, P. He, G. Wang, Y. Shen, C. W. Nan, L. Z. Fan, *Adv. Energy Mater.* **2020**, *10*, 1903376.

[15] S. Xu, Z. Sun, C. Sun, F. Li, K. Chen, Z. Zhang, G. Hou, H. M. Cheng, F. Li, *Adv. Funct. Mater.* **2020**, *30*, 2007172.

[16] S. Xia, X. Wu, Z. Zhang, Y. Cui, W. Liu, *Chem* **2019**, *5*, 753.

[17] Y. Lu, L. Li, Q. Zhang, Z. Niu, J. Chen, *Joule* **2018**, *2*, 1747.

[18] F. Wu, K. Zhang, Y. Liu, H. Gao, Y. Bai, X. Wang, C. Wu, *Energy Storage Mater.* **2020**, *33*, 26.

[19] W. Fan, N. W. Li, X. Zhang, S. Zhao, R. Cao, Y. Yin, Y. Xing, J. Wang, Y. G. Guo, C. Li, *Adv. Sci.* **2018**, *5*, 1800559.

[20] R. Khurana, J. L. Schaefer, L. A. Archer, G. W. Coates, *J. Am. Chem. Soc.* **2014**, *136*, 7395.

[21] F. Liu, T. Li, Y. Yang, J. Yan, N. Li, J. Xue, H. Huo, J. Zhou, L. Li, *Macromol. Rapid Commun.* **2020**, *41*, 2000047.

[22] J. Bae, Y. Li, J. Zhang, X. Zhou, F. Zhao, Y. Shi, J. B. Goodenough, G. Yu, *Angew. Chem. Int. Ed.* **2018**, *57*, 2096.

[23] C. A. Angell, C. Liu, E. Sanchez, *Nature* **1993**, *362*, 137.

[24] Z. X. Wang, W. D. Gao, X. J. Huang, Y. J. Mo, L. Q. Chen, *Electrochem. Solid St.* **2001**, *4*, A148.

[25] a) C. Yi, W. Liu, L. Li, H. Dong, J. Liu, *Funct. Mater. Lett.* **2019**, *12*, 1930006; b) H. Gao, N. S. Grundish, Y. Zhao, A. Zhou, J. B. Goodenough, *Energy Mater. Adv.* DOI: 10.34133/2021/1932952.

[26] K. Kimura, J. Motomatsu, Y. Tominaga, *J. Phys. Chem. C* **2016**, *120*, 12385.

[27] Y. Li, F. Ding, Z. Xu, L. Sang, L. Ren, W. Ni, X. Liu, *J. Power Sources* **2018**, *397*, 95.

[28] Y. Zhao, Y. Bai, Y. Bai, M. An, G. Chen, W. Li, C. Li, Y. Zhou, *J. Power Sources* **2018**, *407*, 23.

[29] Z. Li, J. Mindemark, D. Brandell, Y. Tominaga, *Polym. J.* **2019**, *51*, 753.

[30] Z. Florjańczyk, E. Zygadło-Monikowska, W. Wieczorek, A. Ryszawy, A. Tomaszewska, K. Fredman, D. Golodnitsky, E. Peled, B. Scrosati. *J. Phys. Chem. B* **2004**, *108*, 14907.

[31] L. Chen, L. Z. Fan, *Energy Storage Mater.* **2018**, *15*, 37.

[32] a) J. Hu, P. He, B. Zhang, B. Wang, L. Z. Fan, *Energy Storage Mater.* **2020**, *26*, 283; b) B. Wu, L. Wang, Z. Li, M. Zhao, K. Chen, S. Liu, Y. Pu, J. Li, *J. Electrochem. Soc.* **2016**, *163*, A2248.

[33] R. E. Sousa, J. Nunes-Pereira, J. C. C. Ferreira, C. M. Costa, A. V. Machado, M. M. Silva, S. Lanceros-Mendez, *Polym. Test.* **2014**, *40*, 245.

[34] S. Lou, F. Zhang, C. Fu, M. Chen, Y. Ma, G. Yin, J. Wang, *Adv. Mater.* DOI: 10.1002/adma.202000721.

[35] L. Xu, S. Tang, Y. Cheng, K. Wang, J. Liang, C. Liu, Y. C. Cao, F. Wei, L. Mai, *Joule* **2018**, *2*, 1991.

[36] X. Chen, W. He, L. X. Ding, S. Wang, H. Wang, *Energy Environ. Sci.* **2019**, *12*, 938.

[37] a) F. Lv, Z. Wang, L. Shi, J. Zhu, K. Edström, J. Mindemark, S. Yuan, *J. Power Sources* **2019**, *441*, 227175; b) Q. Xia, Q. Zhang, S. Sun, F. Hussain, C. Zhang, X. Zhu, F. Meng, K. Liu, H. Geng, J. Xu, F. Zan, P. Wang, L. Gu, H. Xia, *Adv. Mater*. DOI: 10.1002/adma.202003524.

[38] Z. Wan, D. Lei, W. Yang, C. Liu, K. Shi, X. Hao, L. Shen, W. Lv, B. Li, Q. H. Yang, F. Kang, Y. B. He, *Adv. Funct. Mater.* **2019**, *29*, 1805301.

[39] B. Zhang, L. Chen, J. Hu, Y. Liu, Y. Liu, Q. Feng, G. Zhu, L. Z. Fan, *J. Power Sources* **2019**, *442*, 227230.

[40] R. J. Chen, Y. B. Zhang, T. Liu, B. Q. Xu, Y. H. Lin, C. W. Nan, Y. Shen, *ACS Appl. Mater. Interfaces* **2017**, *9*, 9654.

[41] Z. Bi, S. Mu, N. Zhao, W. Sun, W. Huang, X. Guo, *Energy Storage Mater.* **2021**, *35*, 512.

[42] a) L. P. Li, W. Y. Liu, H. Y. Dong, Q. Y. Gui, Y. Y. Li, J. P. Liu, *Adv. Mater.* DOI:10.1002/adma.202004959; b) W. Zuo, R. Li, C. Zhou, Y. Li, J. Xia, J. Liu, *Adv. Sci.* **2017**, *4*, 1600539.

[43] a) P. R. Abel, Y. M. Lin, H. Celio, A. Heller, C. B. Mullins, *ACS Nano* **2012**, *6*, 2506; b) Y. Zhou, M. Xue, Z. Fu, *J. Power Sources* **2013**, *234*, 310.

[44] J. Sun, X. Yao, Y. Li, Q. Zhang, C. Hou, Q. Shi, H. Wang, *Adv. Energy Mater.* **2020**, *10*, 2000709.

[45] M. Abreha, A. R. Subrahmanyam, J. Siva Kumar, *Chem. Phys. Lett.* **2016**, *658*, 240.

[46] R. Gonçalves, D. Miranda, A. M. Almeida, M. M. Silva, J. M. Meseguer-Dueñas, J. L. G. Ribelles, S. Lanceros-Méndez, C. M. Costa, *Sustain. Mater. Techno.* **2019**, *21*, e00104.

[47] Z. Hu, F. Xian, Z. Guo, C. Lu, X. Du, X. Cheng, S. Zhang, S. Dong, G. Cui, L. Chen, *Chem. Mater.* **2020**, *32*, 3405.

[48] a) X. Zhang, T. Liu, S. Zhang, X. Huang, B. Xu, Y. Lin, B. Xu, L. Li, C. W. Nan, Y. Shen, *J. Am. Chem. Soc.* **2017**, *139*, 13779; b) W. H. Hou, C. Y. Chen, C. C. Wang, Y. H. Huang, *Electrochim. Acta* **2003**, *48*, 679; c) C. Y. Chiang, Y. J. Shen, M. J. Reddy, P. P. Chu, *J. Power Sources* **2003**, *123*, 222.

[49] a) X. Zhang, S. Wang, C. Xue, C. Xin, Y. Lin, Y. Shen, L. Li, C. W. Nan, *Adv. Mater.* **2019**, *31*, 1806082; b) D. Callegari, S. Bonizzoni, V. Berbenni, E. Quartarone, P. Mustarelli, *Adv. Mater.* **2020**, *32*, 1907375; c) X. Zhang, S. Wang, C. Xue, C. Xin, Y. Lin, Y.Shen, C. W. Nan, *Adv. Mater.* **2020**, *32*, 2000026; d) X. Zhang, J. Han, X. Niu, C. Xin, C. Xue, S. Wang, C. W. Nan, *Batteries & Supercaps*, **2020**, *3*, 876.

[50] Z. Wang, W. Gao, L. Chen, Y. Mo, X. Huang, *J. Electrochem. Soc.* **2002**, *149*, E148.

[51] L. Chen, W. Li, L. Z. Fan, C. W. Nan, Q. Zhang, *Adv. Funct. Mater.* **2019**, *29*, 1901047.

[52] D. Zhou, Y. B. He, R. Liu, M. Liu, H. Du, B. Li, Q. Cai, Q. H. Yang, F. Kang, *Adv. Energy Mater.* **2015**, *5*, 1500353.

[53] A. K. Łasińska, M. Marzantowicz, J. R. Dygas, F. Krok, Z. Florjańczyk, A. Tomaszewska, E. Zygadło-Monikowska, Z. Żukowska, U. Lafont, *Electrochim. Acta* **2015**, *169*, 61.

[54] X. Yu, L. Wang, J. Ma, X. Sun, X. Zhou, G. Cui, *Adv. Energy Mater.* **2020**, *10*, 1903939.

[55] B. Liu, J. E. Boercker, E. S. Aydil, *Nanotechnology* **2008**, *19*, 505604.

[56] J. Chang, Q. Huang, Z. Zheng, *Joule* **2020**, *4*, 1346.

[57] Q. Y. Gui, D. L. Ba, Z. S. Zhao, Y. F. Mao, W. H. Zhu, T. Y. Lei, J. F.Tan, B. H. Deng, L. Xiao, Y. Y. Li, J. P. Liu, *Small Methods* **2019**, *3*, 1800371.

10.1002/ange.202101537

WILEY-VCH

RESEARCH ARTICLE

Entry for the Table of Contents

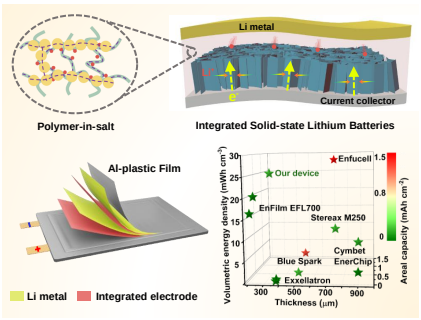

A novel PVDF-HFP-based polymer-in-salt solid electrolyte (PISSE) with high ionic conductivity at room temperature and a solid-state lithium battery (SSLB) with 3D fully infiltration of PISSE are developed. The integrated device simultaneously achieves maximized interfacial contact and electrochemical and mechanical stability, presenting high performance close to that with liquid electrolyte. With packaging two integrated SSLB units in series, a 3.7 V pouch cell is fabricated, exhibiting robust flexibility and brilliant safety.